ACS OMEGA

ACS AUTHORCHOICE

http://pubs.acs.org/journal/acsodf

Article

PLLA Porous Microsphere-Reinforced Silk-Based Scaffolds for Auricular Cartilage Regeneration

Yan Zeng, Xiaokai Li, Xia Liu, Yuzhou Yang, Zhimin Zhou,* Jincai Fan,* and Haiyue Jiang*

Cite This: *ACS Omega* 2021, 6, 3372−3383

Read Online

ACCESS | Metrics & More | Article Recommendations | Supporting Information

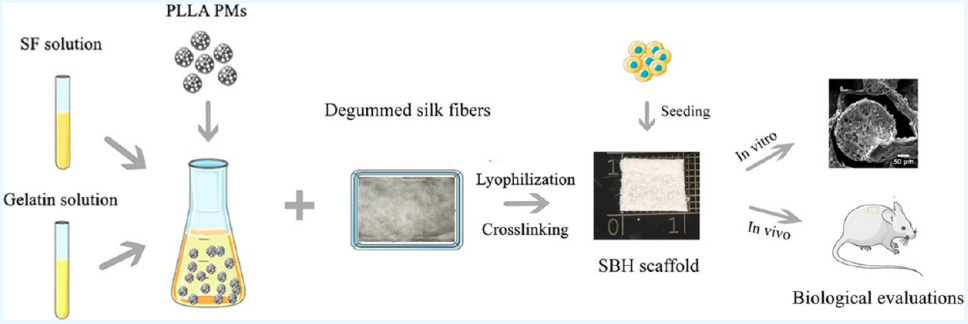

ABSTRACT: Microtia, frequently encountered in plastic surgery practice, is usually corrected by auricular reconstruction with prostheses or autologous cartilages. In recent decades, however, cartilage tissue engineering has been emerging as a promising alternative for its minimal invasion and low immunogenicity. As a critical factor for tissue engineering, scaffolds are expected to be sufficiently porous and stiff to facilitate chondrogenesis. In this work, we introduce novel poly-L-lactic acid (PLLA) porous microsphere-reinforced silk-based hybrid (SBH) scaffolds with a multihierarchical porous structure. The scaffolds are fabricated by embedding PLLA porous microspheres (PMs) into a blending matrix of silk fibroin (SF) and gelatin solution, followed by mixing with a degummed silk fiber mesh and freeze-drying process. Through adjusting the amount of PLLA PMs, the mechanical strength approximates to natural cartilage and also balanced physical properties were realized. Biological evaluations of SBH scaffolds, both in vitro and in vivo, were conducted and PM-free plain silk-based (PSB) scaffolds were applied as control. Overall, it suggests that the incorporation of PLLA PMs remarkably improves mechanical properties and the capability to promote chondrogenesis of SBH scaffolds, and that SBH scaffolds appear to be a promising construct for potential applications in auricular cartilage tissue engineering and relevant fields.

1. INTRODUCTION

Microtia is a congenital auricular abnormality, which induces psychological and cosmetic issues during growth of children.[1] To date, utilization of auricular prostheses and autologous cartilages is still a main approach to reconstructing external ear in plastic surgery.[1−3] However, complications like extrusion and rejection frequently occur and have to be concerned when prostheses are applied. Additionally, donor-site morbidity and the skills required for surgeons are the main limitations for autologous rib cartilage technique, which is still the gold standard for microtia treatment. To address these issues, cartilage tissue engineering was proposed and expected to make breakthroughs for external ear reconstruction.[2−4] It is widely recognized that the attachment, proliferation, and differentiation of seeding cells on polymeric scaffolds largely depend on the distinct features of scaffolds, such as porosity, pore size, surface topology, mechanical properties, and degradation profile, in addition to factors like seeding cell category and growth factor signals.[5−9] Especially, adequate mechanical strength is in favor of maintaining the integrity and morphology of newly formed engineered tissue.[10,11] Therefore, it is necessary to explore a polymeric scaffold with desired mechanical features in auricular cartilage tissue engineering.

In general, to meet the required mechanical strength for tissue regeneration, chemical cross-linking or physical composition strategy is routinely considered in the design of reinforced scaffolds. Among various attempts, fiber-reinforced composites have become intensively studied for bone and cartilage regeneration.[12−17] In previous reports, silk microfiber-reinforced composites offered advantages over their fiber-free counterparts and displayed tunable properties including compressive strength, surface roughness, and porosity, as fiber lengths or silkworm species altered.[14,15] However, it

Received: December 3, 2020
Accepted: January 13, 2021
Published: January 25, 2021

https://dx.doi.org/10.1021/acsomega.0c05890
ACS Omega 2021, 6, 3372−3383

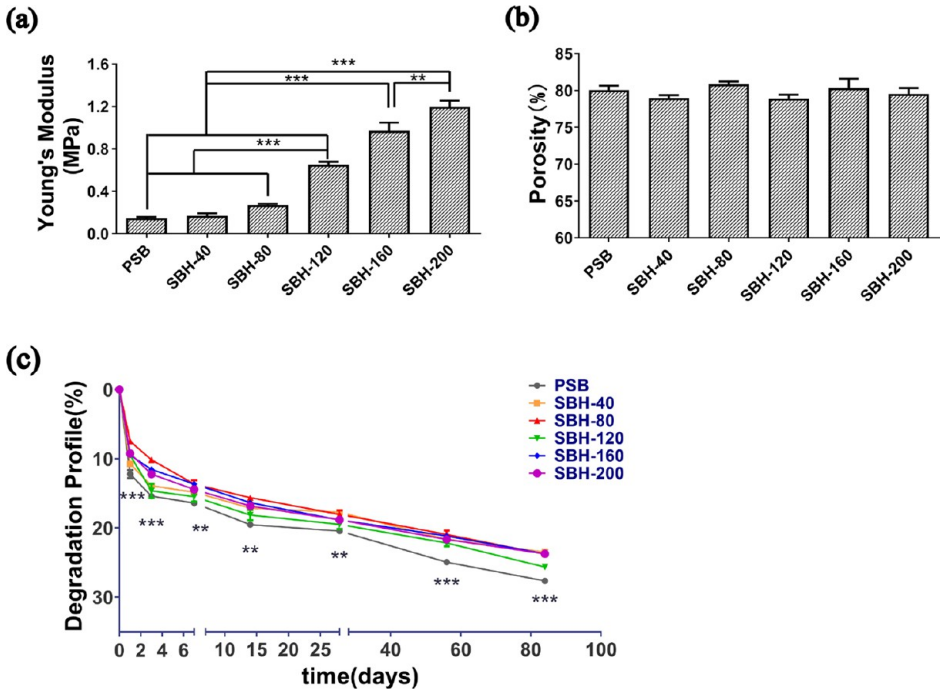

Figure 1. Physical characterizations of PSB and SBH scaffolds: Young's modulus for compression (a), porosity (b), and degradation rate (c) of PSB and SBH scaffolds. The number of SBH represents the amount (mg) of PLLA microspheres used in scaffolds ($n \geq 3$, $^{*}P < 0.05$, $^{**}P < 0.01$, $^{***}P < 0.001$).

should be noted that the short length of silk microfibers limits their interconnection as an integral structure, suggesting that the role of microfibers is more as fillers for bulk matrix than as supporting structures. In contrast to microfibers of silk, full-length degummed silk fibers can act as the loading transferee to reinforce silk fibroin (SF) porous scaffolds, as well as regulate the degradation profile to realize better structural integrity for the ingrowth of newly formed tissue.[16,17] Furthermore, isotropic polymeric microspheres, generally used as bioactive molecule delivery vehicles in composite scaffolds, were found to improve the mechanical performance of the whole construct, similar to anisotropic silk fibers or microfibers.[18−22] Apart from their mechanical properties, polylactic acid (PLA) or poly[lactic-*co*-(glycolic acid)] (PLGA) porous microspheres (PMs), with their high porosity and large surface area, also attracted extensive attention for their biological applications as inhaled drug-delivery vehicles or cell carriers in injectable fillers.[23−25] Recent studies even showed that PLGA PMs are used as three-dimensional (3D) bio-ink, which not only facilitate adherence and proliferation of seeding cells but also provide high anticompression strength for the integral hybrid scaffold.[26] In fact, since first reported in 1997, PLA-coated polyglycolic acid (PGA) nonwoven mesh has been regarded as one of the most promising materials for auricular cartilage tissue engineering due to its excellent mechanical properties and plasticity, and thus has been applied in clinical scenes.[2,27] Despite their satisfactory performance in chondrogenesis promotion and morphology maintaining, PLA and PGA were not widely applied because of the unexpected immunoreaction caused by their acidic catabolite in immunocompetent animals. A possible solution from the biological perspective might be bone marrow mesenchymal stem cells (BMSCs), which could suppress in vivo inflammation aroused by PLA/PGA scaffolds via increasing M2 polarization of macrophages.[28] Alternatively, a prevalent method in chemical view for optimized scaffolds is to reduce the amount of lactic acid-based polymers or make a composite with other biomaterials, such as silk and gelatin.[29] Therefore, inspired by the studies mentioned above and the "steel-bar-reinforced concrete" structure in architecture, we designed a scaffold with optimized mechanical features and a multihierarchy porous structure that applied full-length degummed silk mesh as "steel bars" while a mixture of SF, gelatin, and poly-L-lactic acid (PLLA) PMs as "concrete" for auricular cartilage regeneration.

In the present study, we prepared the hybrid scaffolds by embedding PLLA PMs in a porous silk-based matrix. Physicochemical features such as mechanical strength, porosity, and degradation rate were investigated to optimize the amount of PMs. The in vitro biocompatibility of the as-prepared scaffolds was investigated with porcine auricular chondrocytes by live/dead staining, CCK-8 assays, and quantitative polymerase chain reaction (qPCR), while the in vivo cartilage formation was also evaluated by subcutaneous implantation in a nude mice model. For all of the tests, plain silk-based porous (PSB) scaffolds without PLLA PMs were applied as control.

2. RESULTS AND DISCUSSION

2.1. Physical Characterizations. The mechanical properties of PSB scaffolds, as shown in Figure 1a, e.g., Young's modulus (0.15 ± 0.03 MPa), were approximately equal to those of freeze-dried SF porous scaffolds reported in previous studies.[16,17] The mechanical strength of silk-based hybrid (SBH) scaffolds proves to be reinforced by the incorporation of PLLA PMs, especially when the amount reaches 120 mg and above. The Young's moduli of SBH-120, SBH-160, and SBH-200 were at least 3-fold larger than those of PSB scaffolds, and the value increased with the amount of PM augments. Among them, the SBH-200 scaffolds showed a value of 1.20 ± 0.15 MPa, in the native auricular cartilage range,[30,31] which is

https://dx.doi.org/10.1021/acsomega.0c05890
ACS Omega 2021, 6, 3372−3383

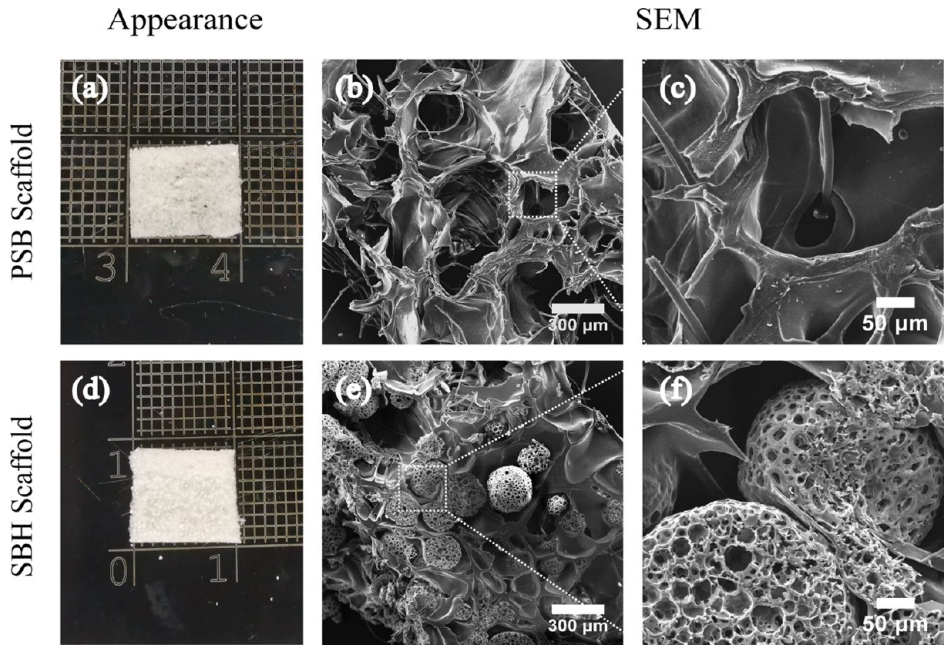

Figure 2. Gross appearance (a, d) and SEM images (b, c, e, f) of PSB (a−c) and SBH (d−f) scaffolds.

significantly higher than the value of all of the other tested scaffolds. As reported in previous studies, by inducing silk fibers into nature-originated porous scaffolds, the compression modulus could rise remarkably, which reached 20−400 kPa in the case of microfibers[13,14] and 15−750 kPa in the case of full-length fibers.[16] Similarly, the incorporation of PMs improved the Young's modulus of porous scaffolds to the range of 5−130 kPa.[22,32] However, there is still a gap in compression modulus between the above-mentioned studies and the value of SBH scaffolds and native cartilage. Thus, compared to previous designs, SBH scaffolds are more likely to provide a mechanically stable substrate for seeding chondrocytes and subsequently facilitate better chondrogenesis results.

Furthermore, PSB scaffolds revealed a high porosity of around 80.1 ± 1.0% and the incorporation of PLLA PMs had hardly any effects on the porosity of scaffolds; all tested samples showed a measurement ranging from 78.2 to 82.6%, and no statistically significant difference is observed among the groups (Figure 1b). The degradation of PSB scaffolds and SBH scaffolds showed a similar tendency. Drastic degradation took place in the first 3 days. As a result, by day 3, the degradation rate of each group reached 10−15%. Afterward, the scaffolds degraded slowly and steadily until day 84, by which the ultimate degradation rate was within 30%. During the whole tested period, all SBH scaffolds degraded slower than PSB scaffolds, regardless of the amount of PMs, and the difference is statistically significant. Except for SBH-120, the difference of degradation rate among SBH scaffolds was hardly remarkable, especially in the late period of the test (Figure 1c).

In general, a promising scaffold is expected to be equipped with adequate mechanical strength and appropriate degradation rate to maintain integrity and morphology of newly formed engineered tissue,[3] especially when it is applied in the field of plastic surgery, the primary task of which is appearance reconstruction. In addition, a highly porous structure facilitating cell proliferating and migrating is also essential for chondrocytes phenotype maintaining and chondrogenesis.[7] Therefore, based on the results of physical properties, the SBH-200 sample, characterized with a high mechanical strength and adequate porosity, as well as a moderate degradation rate, was selected for further studies.

2.2. Gross Appearance and Scanning Electron Microscopy (SEM) Images. As shown in Figure 2a, the PM-free PSB scaffolds presented a white and spongy-like appearance. Further detected by SEM, the PSB scaffolds demonstrated a highly interconnected porous three-dimensional structure with a trabecular-like network and unrepresentative spherical pores. The pores were heterogeneous, diameters of which range from 300 to 500 μm. The degummed silk fibers were embedded and randomly distributed all over the SF and gelatin matrices (Figure 2b,c). SBH scaffolds displayed a similar gross appearance to the PSB ones, but with less transparency and diffused white dots, which indicated the embedded PLLA PMs (Figure 2d). The SEM images of SBH scaffolds also exhibited a highly porous structure, but some of the trabecular-formed pores were filled by PLLA PMs. These PMs, with diameter 245 ± 35 μm and pore size 27 ± 4.8 μm, maintained their spherical shape and integrity after fabrication, equipping the scaffolds with a multihierarchy porous structure for potential cell migrating (Figure 2e,f). In the literature, the average diameters of incorporated microspheres were much smaller than the pore sizes of their corresponding scaffolds,[22,32] while PLLA PMs applied in this study have an approximate diameter with matrix-formed pores. The latter proved to perform much better in mechanical improvement of corresponding scaffolds. Possibly, with a larger volume, the relatively robust PMs are more facilitated to bear loading transferred from the matrices, as more contact points and directions could be realized.

Furthermore, the debate on whether large or small pores of scaffolds benefit chondrogenesis remains controversial in the literature. In general, researchers tend to confirm the advantage of larger pores in better cell migration, nutrition diffusion, mass exchange, and signal transduction brought about by high permeability.[7−9] The phenomenon that pores smaller than 150 μm in diameter are inclined to hinder chondrocytes ingrowth

https://dx.doi.org/10.1021/acsomega.0c05890
ACS Omega 2021, 6, 3372−3383

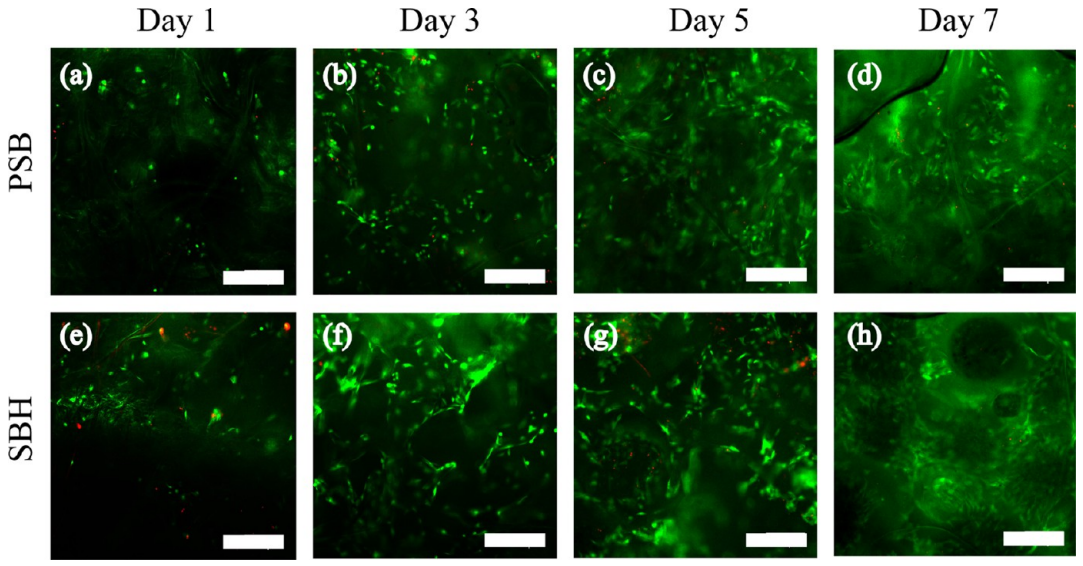

Figure 3. Live/dead staining images of PSB (a–d) and SBH (e–h) scaffolds on days 1, 3, 5, and 7 after chondrocytes seeding (scale bar: 300 μm).

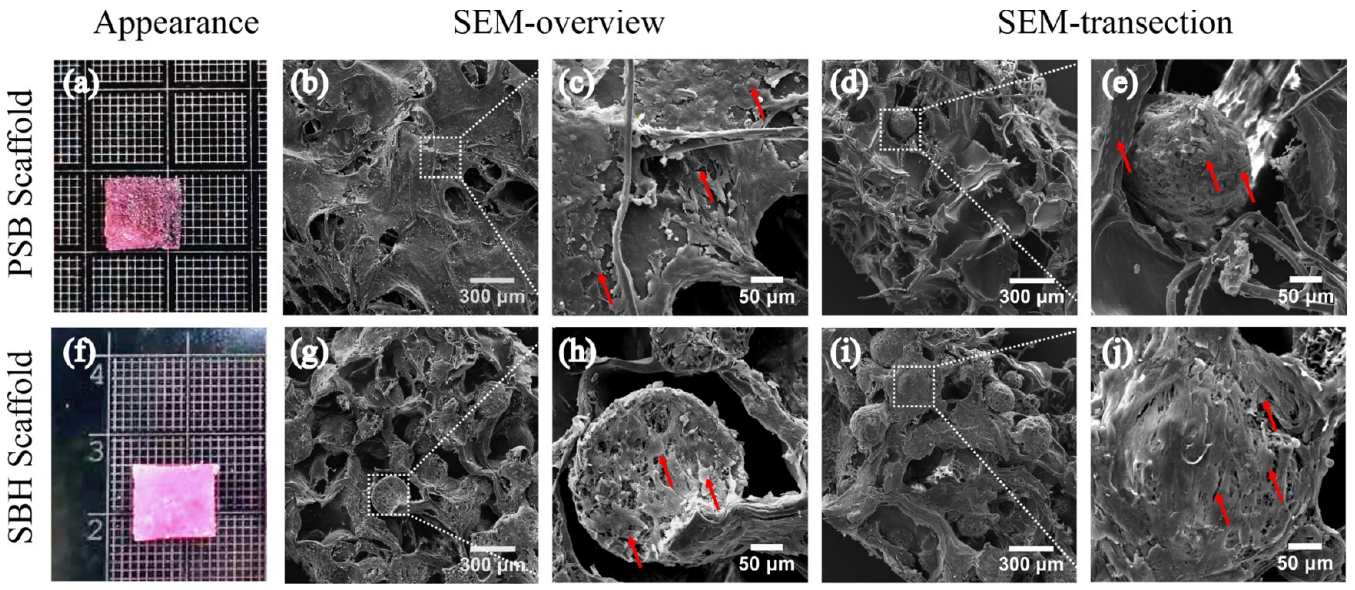

Figure 4. Gross appearance (a, f) and SEM images (b–e,g–j) of cell-laden PSB (a–e) and SBH (f–j) scaffolds after cultivation in vitro for 4 weeks. The white squares represent the regions corresponding to the magnified SEM images. The red arrows represent the polygonal-shaped chondrocytes encapsulated in ECM, which either distribute along pore walls or aggregate as bulk in pores in the PSB group (b–e), and proliferates onto or into PLLA PMs in the SBH group (g–j).

and phenotype maintaining was repeatedly confirmed.[33] A range between 250 and 500 μm was even recommended by some scholars for the design of porous scaffolds.[8] However, the opposite tendency that scaffolds with smaller pores performed better than those with larger pores was also concluded by some studies.[34] The potential reason might be attributed to the low permeability and oxygen stress caused by smaller pores for natural cartilage is much less metabolically active and permeable than bone or vascularized soft tissues.[35,36] Therefore, in the present study, SBH scaffolds are designed and confirmed to be equipped with a multihierarchy and highly interconnected porous structure, which is expected to provide high permeability for cell migration and mass exchange in the early stage of cultivation and induce lower permeability as chondrocytes migrate into PMs with smaller pores.

On the other hand, although PLLA PMs served as qualified scaffolds for cartilage regeneration by providing extra surface and proper conditions for neocartilage formation, their hydrophobic surface was believed to hinder cell adhesion post seeding and subsequent chondrogenesis. In SBH's design, the hydrophobicity of PLLA PMs is prospected to be ameliorated by high-cell-affinity SF and gelatin matrices that encapsulates them. Gelatin and SF, both natural materials with excellent biocompatibility and low immunogenicity,[37−39] are believed to facilitate chondrocyte adhesion, growth, and migration into embedded PMs.

Thus, from the perspective of microscopic structure, SBH scaffolds are expected to perform equally well with the PSB ones at the early stage of cultivation for comparable porosity and cell affinity, and even better at the later stage for their multihierarchy porous structure.

https://dx.doi.org/10.1021/acsomega.0c05890
ACS Omega 2021, 6, 3372−3383

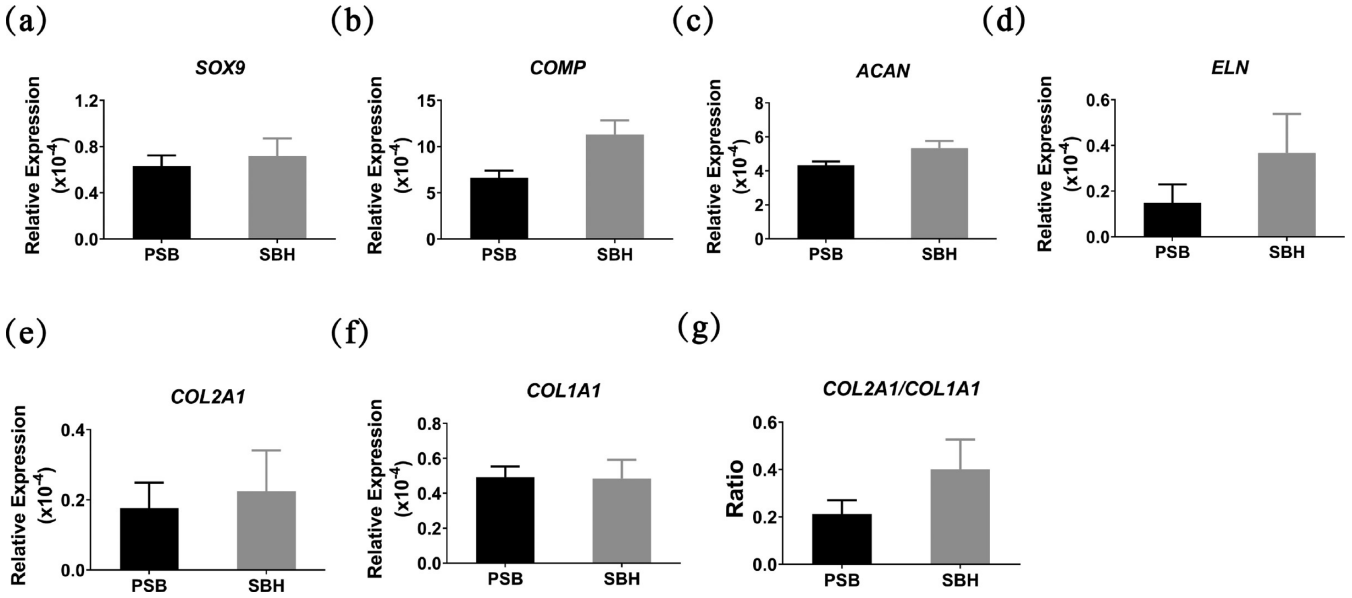

Figure 5. Relative expression of chondrogenesis-related genes of seeded cells on PSB and SBH scaffolds after in vitro cultivation for 4 weeks, measured by real-time PCR (a–g).

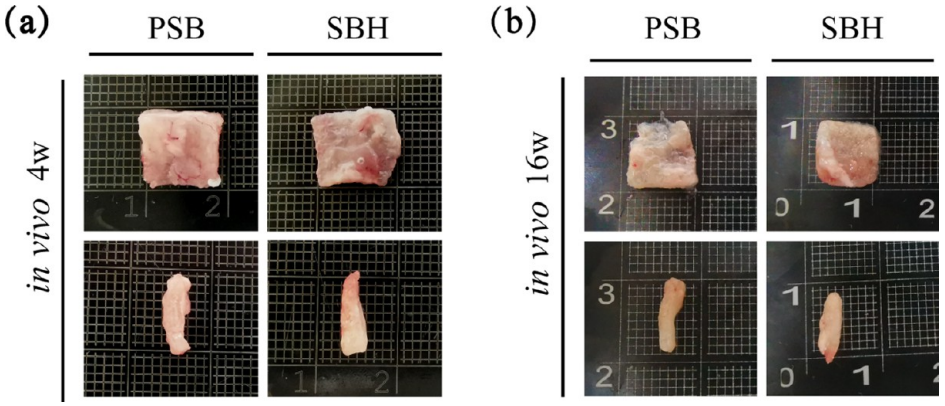

Figure 6. Gross appearance of cell-laden PSB and SBH scaffolds after cultivation in vitro for 4 weeks and in vivo for another 4 weeks (a) and 16 weeks (b).

2.3. *In Vitro* Biocompatibility Evaluations. Cell attachment and viability of both scaffolds were determined through live/dead staining on days 1, 3, 5, and 7 after seeding. On day 1, the cells showed similar adhesion on PSB and SBH scaffolds as they show roughly equal densities of green signals, while more red stains were also detected on SBH scaffolds (Figure 3a,e). On days 3 to 7, green stains gradually increased and distributed more homogeneously on both scaffolds, revealing that chondrocytes proliferated and migrated well (Figure 3b–d,f–h). We did not observe significant differences of proliferation between PSB and SBH scaffolds during this period. CCK-8 assays were performed to further evaluate the metabolic activity and proliferation of cells up to 21 days post seeding. The cells presented a significant increase of metabolic activity over the 21 days of culturing, especially in the latter half of the period ($P < 0.001$), indicating the excellent biocompatibility of both scaffolds (Figure S1). For each time point, no significant difference in cell viability can be observed between the two groups, consistent with the live/dead staining results (Figure 3). In brief, in the first 3 weeks of in vitro cultivation, PSB and SBH scaffolds are comparably capable of providing a favorable environment for chondrocytes attachment, growth, and migration as expected.

2.4. Morphology Observation of Cell-Laden Scaffolds. On 28 days post cell seeding, the PSB scaffolds displayed no remarkable variation in shape and volume but became denser and less transparent compared to cell-free samples (Figure 4 a). Similar changes were also found in SBH scaffolds (Figure 4f). The SEM images of the cell-laden scaffolds exhibited that a large amount of cells adhered on the surface and penetrated into pore structures of both scaffolds, but with different distribution patterns. For PSB scaffolds, chondrocytes were found either distributing along flake-like walls and silk fibers or aggregating as bulk in pores (Figure 4b–e). While for SBH scaffolds, a large number of chondrocytes were observed to proliferate onto and into PLLA PMs (Figure 4g–j). In addition, chondrocytes on two scaffolds both presented a polygonal shape and were encapsulated in abundant extracellular matrix (ECM), indicating little dedifferentiation tendency and excellent ECM secretion capability of these cells. Thus, during the 4-week in vitro cultivation period, both PSB and SBH scaffolds were considered to provide an appropriate environment for

https://dx.doi.org/10.1021/acsomega.0c05890
ACS Omega 2021, 6, 3372–3383

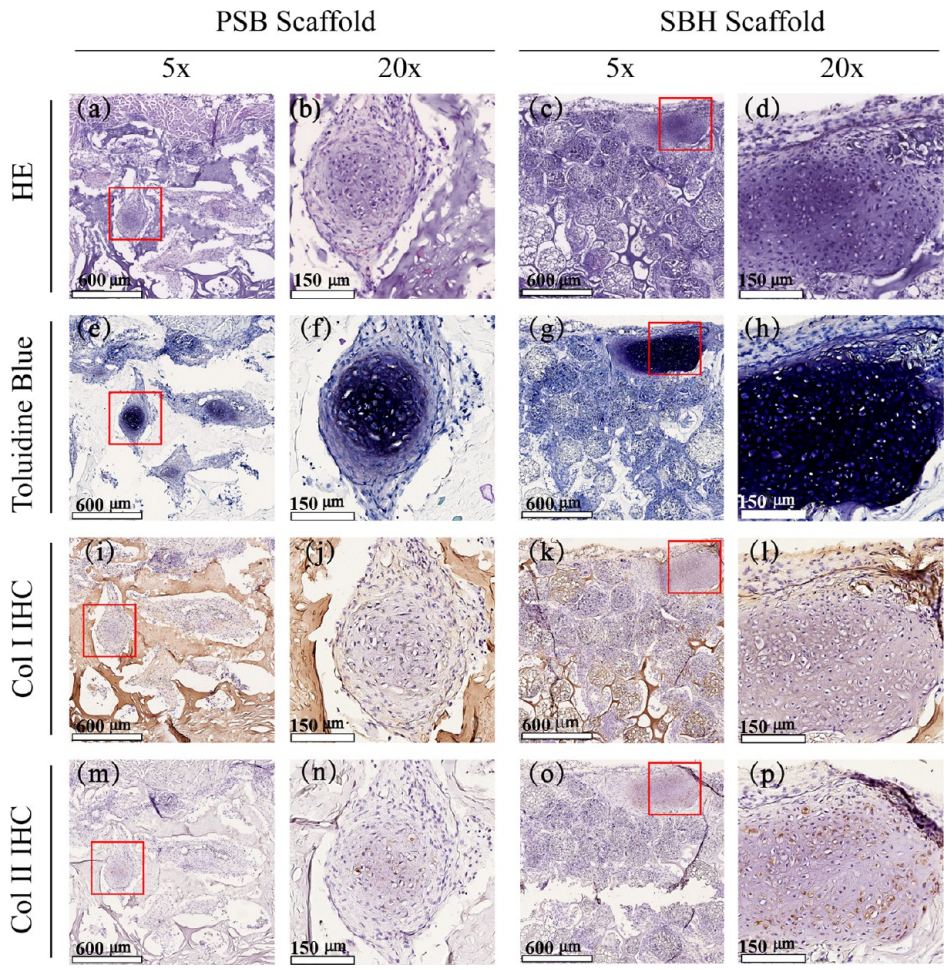

Figure 7. HE (a–d) and toluidine blue (e–h), as well as Col I (i–l) and Col II (m–p) immunohistochemical staining images of cell-laden PSB (left) and SBH (right) scaffolds after cultivation in vitro for 4 weeks and in vivo for another 4 weeks. The red squares represent the regions corresponding to the magnified stained images.

chondrocytes proliferation, migration, and phenotype maintaining.

2.5. Chondrogenesis-Related Gene Expression. The expression levels of chondrogenesis-related gene estimated by real-time PCR demonstrated that SBH scaffolds had a slight advantage over PSB scaffolds in all tested genes except COL1A1 (Figure 5a–f). And the ratio of *COL2A1/COL1A1* was also a little higher in the SBH group (Figure 5g), which, as mentioned in the literature, indicates a potentially less dedifferentiation and more chondrogenesis tendency.[40−42] However, all of the differences above were not statistically significant, although all of the results presented a consistent trend that slightly better chondrocytes phenotype maintaining and ECM production were likely to take place in the SBH group. The demonstrations above confirm the similar capability of both scaffolds to serve as cartilage tissue engineering scaffolds during the 4-week in vitro cultivation period.

2.6 *In Vivo* Evaluation of Chondrogenesis. After in vivo cultivation for 4 weeks, harvested samples of both groups did not change much in shape and size and a thin capsule of soft tissue with vessels could be observed on their surface (Figure 6a). However, the samples explanted after 16 weeks presented an obvious shrink in size, regardless of the group. A large scale of degradation was observed in the PSB group and the remaining part of the samples had hardly a regular shape and were mechanically unstable. On the contrary, the SBH samples still kept integral and stiff despite the degradation, and some newly formed cartilage tissue could even be detected on the surface (Figure 6b).

To further estimate and compare neocartilage formation of two scaffolds, histological analyses were conducted among explanted samples after in vivo cultivation. Figure 7 demonstrates hematoxylin and eosin (H&E), toluidine blue, as well as Col I and Col II immunohistochemistry (IHC) staining images after the 4-week period in vivo cultivation. H&E staining of PSB scaffolds shows well-defined cartilage-like tissue distributed homogeneously in pores, with a relatively loose texture. Chondrocytes with lacuna structures could be detected in the central part of the bulk (Figure 7a,b), consistent with the purple-dyed area in toluidine blue staining images (Figure 7e,f), which indicates a decent deposition of glycosaminoglycan (GAG), one of the main components of cartilage ECM. Contrary to the PSB ones, the H&E staining images of SBH scaffolds present an uneven distribution mode. Chondrocytes tend to accumulate in high density in the marginal part of scaffolds and around PMs. A large amount of PMs were filled by chondrocytes and their ECM; meanwhile, unoccupied PMs could also be frequently detected. In the chondrocyte-accumulating area, which is larger in the SBH group than in control, delicate cartilage lacunas and denser basophilia dyes could be observed via H&E staining images

https://dx.doi.org/10.1021/acsomega.0c05890
ACS Omega 2021, 6, 3372−3383

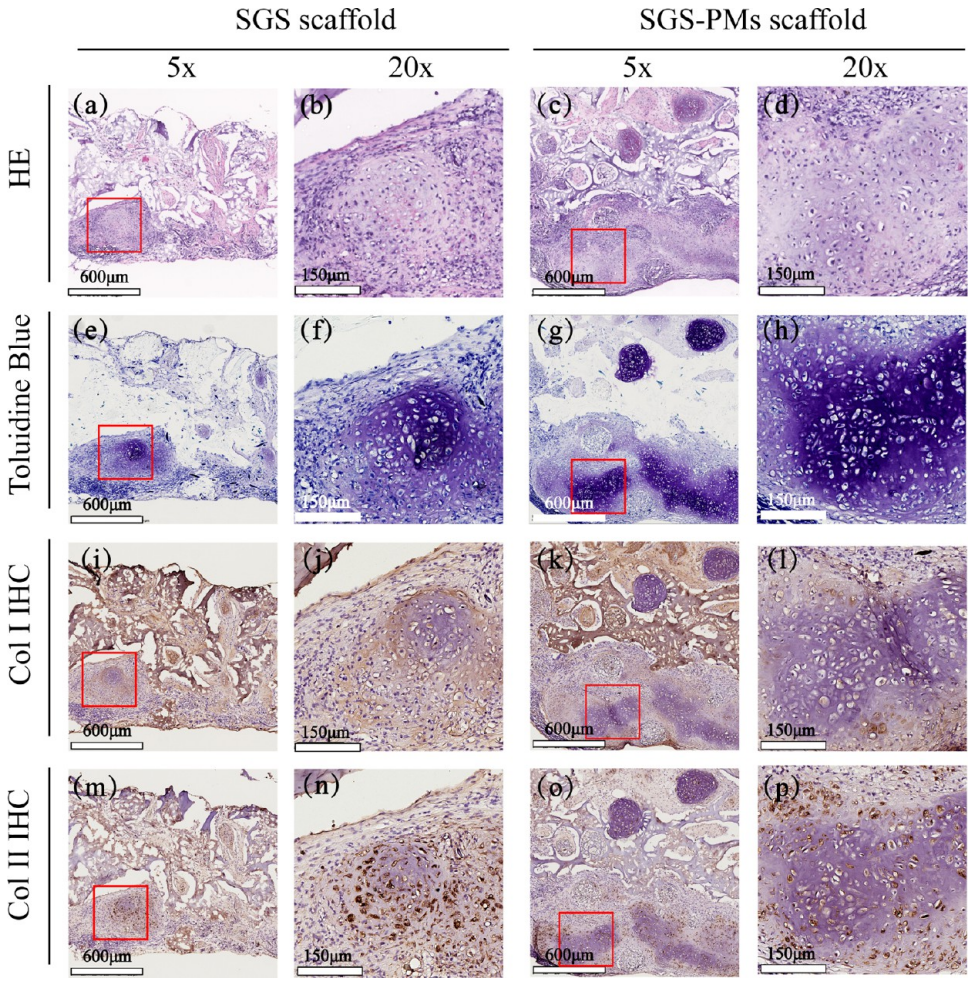

Figure 8. HE (a–d) and toluidine blue (e–h), as well as Col I (i–l) and Col II (m–p) immunohistochemical staining images of cell-laden PSB (left) and SBH (right) scaffolds after cultivation in vitro for 4 weeks and in vivo for another 16 weeks. The red squares represent the regions corresponding to the magnified stained images.

(Figure 7c,d), while remarkable deposition of GAG and type II collagen could also be detected via toluidine blue and Col II staining images (Figure 7g,h,o,p). In addition, compared to the PSB ones, SBH scaffolds show more positive dyes of type II and less of type I collagen, indicating a higher quality of neocartilage tissue (Figure 7i–p).

In comparison to the 4-week ones, the images of 16-week harvested SBH samples demonstrate a significant increase in cell number and staining intensity. Besides the marginal area, the central part of the SBH scaffolds is also observed to be filled with chondrocytes (Figure 8c,d), as well as dense GAG and Col II depositions (Figure 8g,h,o,p). Furthermore, compared to their PM-free counterparts, SBH scaffolds exhibit larger volumes of neocartilage bulk, more GAG and Col II dyes, as well as less Col I deposition (Figure 8e–h,i–l,m–p). In addition, we also observe a much thicker transaction in the SBH group, indicating a tendency of more neocartilage formation and less structure collapse (Figure 8a–d). Thus, through histological analyses, SBH scaffolds are considered to perform better than the PM-free PSB ones after 16-week in vivo cultivation.

Taken together, in the early stage of culturing, the cell viability and proliferation, reflected by live/dead staining and CCK-8 assays, were equally desirable in both groups. Over time, the gap between these two scaffolds in chondrogenesis capability gradually emerged and enlarged. After in vitro cultivation for 4 weeks, SBH scaffolds revealed a slight advantage over the PSB ones in the expression of chondrogenesis-related genes, though the difference was not significant. Subsequently, the differences of cartilage formation and Col II production between SBH and PSB scaffolds, estimated by histological analyses, arose after in vivo cultivation for 4 weeks and then got even more remarkable after in vivo cultivation for another 12 weeks. Therefore, it can be postulated that SBH scaffolds are more equipped with the capability to maintain morphology and to promote cartilage formation than the PSB ones, especially when it is estimated from a long-term view.

By comparing the structures of SBH and PSB scaffolds, an association between embedded PMs and better cartilage formation outcomes might be inferred. SEM images demonstrated the phenomenon that seeded chondrocytes on SBH scaffolds tended to migrate onto and into PMs due to hierarchical pore size as expected. Similarly, round and likely PM-centered neocartilage bulk can be observed in the histological images of in vivo cultivation for 16 weeks, which indirectly verifies the chondrogenesis promotion capability of PLLA PMs. One of the possible mechanisms is that relatively isolated space within PMs, accompanied with increasingly aggregated ECM, created an environment with lower oxygen tension, which is more approximate to natural cartilage

https://dx.doi.org/10.1021/acsomega.0c05890
ACS Omega 2021, 6, 3372–3383

microenvironment than the larger pores outside. In fact, the increase of oxygen is even related to diseases such as osteoarthritis.[6] Another potential mechanism lies in the mechanical improvement brought by PLLA PMs to the whole construct. The mechanical properties of scaffolds were confirmed to influence the behaviors of seeding cells and subsequent tissue formation process in the literature.[11,35] As for the situation of auricular regeneration, scaffolds with comparable stiffness to natural cartilage are more likely to withstand skin tension, maintain the original shape, and provide a stable substrate for laden chondrocytes to proliferate and migrate, which is fundamental to neocartilage formation. In addition, frequent cell−cell reactions are more likely to happen in narrow space within PMs, which might contribute to better chondrogenesis as well.[34]

Therefore, the newly designed SBH scaffolds are confirmed by both in vitro and in vivo estimations to be promising in cartilage tissue engineering, which might contribute to the reconstruction of auricles, as well as other structures such as eyelids and nasal alars. Traditionally, the reconstruction of these structures is realized by transplantation of autologous cartilage or using prostheses. Tissue engineering, constructing cartilage-like tissue by proliferating chondrocytes, provides alternative supporting materials for regeneration at much less damage and lower immunogenicity. Furthermore, by adjusting the ratio or amount of silk fibers and PMs, SBH scaffolds are also likely to reach mechanical demands for some cosmetic applications, such as augmentation of foreheads, chins, and zygomatic area. Generally, the potential applications of SBH scaffolds in plastic surgery are worth anticipating. Nevertheless, the latent immunogenicity of composite SBH scaffolds still exists and possibly has effects on the neocartilage formation in immunocompetent animals, which is of necessity to be verified by further investigations.

3. CONCLUSIONS

In summary, we designed a structurally and functionally optimized hybrid scaffold by embedding PLLA PMs into a silk-based porous structure. By adjusting the amount of PMs, the scaffolds were equipped with multihierarchy porous structure and comparable mechanical strength to natural auricular cartilage. The newly designed scaffolds present better performance in chondrogenesis promotion capability than their PM-free counterparts and are promising in cartilage tissue engineering, especially in plastic surgery-related fields.

4. EXPERIMENTAL SECTION

4.1 Materials. Poly-L-lactic acid (PLLA, M_w: 50 000, Daigang Biomaterial, Jinan, China); methylene chloride (Fengchuan Chemical Reagent Co., Tianjin, China); ammonium bicarbonate (Adamas-β, Shanghai, China); poly(vinyl alcohol) (PVA, Sinopec Chongqing Svw Chemical Co., Chongqing, China); NaOH (Fengchuan Chemical Reagent Co., Tianjin, China); and degummed silk and SF (Beijing Sinolactide Medical Technology Company, China). Gelatin (Macklin, Shanghai, China); carbodiimide (EDC) (Aladdin, Shanghai, China); type IV collagenase (Sigma-Aldrich, MO); high-glucose Dulbecco's modified Eagle's medium (H-DMEM, Gibco, CA); fetal bovine serum (FBS, Gibco, CA); penicillin−streptomycin−neomycin antibiotic mixture (PSN, Gibco, CA); LIVE/DEAD Viability/Cytotoxicity Kit (Thermo Fisher, CA); CCK-8 solution (Beyotime, Shanghai, China); TRIzol reagent (Thermo Fisher, CA); Go Taq qPCR and RT-qPCR systems (Promega); SYBR Green Kit (Roche, Germany); 4% paraformaldehyde solution (Beyotime, Shanghai, China); sucrose (Sigma, MO); optimum cutting temperature (OCT) compound (Sakura, Japan); anti-collagen I antibody (Abcam, U.K.); anti-collagen II antibody (Abcam, U.K.); secondary antibody (Solarbio, Beijing, China); and DAB detection kit (Solarbio, Beijing, China).

4.2. Fabrication of Silk-Based Scaffolds Containing PLLA PMs. The PLLA PMs were prepared using a double-emulsion solvent evaporation method. Briefly, 200 mg of PLLA was dissolved in 8 mL of methylene chloride. Afterward, the initial emulsion was prepared by adding 2.5 mL of ammonium bicarbonate aqueous solution (1%, w/w) to the above-mentioned PLLA solution under stirring conditions. The initial emulsion was poured into a 1% (w/w) PVA aqueous solution to form the double emulsion ($W_1/O/W_2$), which was kept magnetically stirred at room temperature for 3 h, promoting volatilization of the organic solvent. PLLA PMs were then collected, washed thrice with distilled water, and resuspended in a 0.1 mol/L NaOH solution, and allowed to stand at room temperature for 20 min. After these steps, PMs were washed another three times, collected, freeze-dried, and preserved under dry and dark conditions.

The SF and gelatin aqueous solution was obtained, respectively, and mixed to a blended solution. The as-prepared PLLA PMs mentioned above were then weighed and added to the solution, to form a 15 mL of system containing 45 mg of silk fibroin, 1.35 g of gelatin, and a certain amount of PMs (0, 40, 80, 120, 160, and 200 mg). The silk-based hybrid scaffolds containing 0 mg of PLLA PMs were set as the PSB scaffolds and also the control group. For all of the groups, the blends were poured into a mold filled with degummed silk mesh and vacuum freeze-dried. Afterward, the constructs were immersed in 1% (w/v) EDC for 8 h to achieve cross-linking, followed by washing in distilled water three times. The scaffolds were then cut into cuboids (10 mm × 10 mm × 2 mm) for further study.

4.3. Physical Properties Evaluation. *4.3.1. Mechanical Properties.* The mechanical properties of scaffolds were measured by a universal material testing machine (INSTRON). The cuboid-shaped scaffolds were prepared by incubating in phosphate-buffered saline (PBS) at 37 °C for 30 min. Before the test, the scaffolds were gently wiped. In addition, the length, width, and height of each scaffold were carefully measured for further calculation. The compression speed was 1 mm/min, and tests were run until a 50% reduction in sample height had been achieved. The results were represented by Young's modulus for compression (MPa).

4.3.2. Porosity Measurement. The porosity of each scaffold was measured by liquid displacement test. Briefly, the scaffolds were cut to cuboids and the volumes of scaffolds were calculated by multiplying their length, width, and height, which was recorded as V_0. The weight of each scaffold was also measured and denoted as m_0. Then, the scaffolds were immersed in absolute ethanol under negative pressure for a few minutes, followed by another 2 h soaking at normal atmospheric pressure. The scaffolds were then taken out, wiped gently to remove liquid on the surface, and weighed instantly, which was denoted as m_1. The volumes of pores in scaffolds were calculated by the weight of ethanol taking up the space using the equation below (the density of ethanol is 0.789 mg/mL under room temperature).

https://dx.doi.org/10.1021/acsomega.0c05890
ACS Omega 2021, 6, 3372−3383

Table 1. Primer Sequences Used for Real-Time PCR

gene	primer sequence	GenBank no.
SOX9	F: CAAACTCTGGAGACTGCTGAATGA	NM_213843.2
	R: TGGCGTTGGGAGAGATGTG	
ACAN	F: CACTGTTACCGCCACTTC	NM_001164652.1
	R: GTCGTTCAAGCCAATCCA	
COL2A1	F: CACGCTCAAGTCCCTCAACA	XM_021092611.1
	R: CATGGCGTCCAAAGTGCATC	
COL1A1	F: AGACATCCCACCAGTCACCT	XM_021067153.1
	R: TCACGTCATCGCACAACACA	
ELN	F: CCTGGCTTTGGACTGTCTCC	NM_001315724.2
	R: TCACTTTCTCTTCCGGCCAC	
COMP	F: AGCGACCAAGACAAGGATGG	XM_003123527.3
	R: AGTCTTGTTGGGCGCTGTTA	
GAPDH	F: GTATGATTCCACCCACGGCA	NM_001206359.1
	R: CACCCCATTTGATGTTGGCG	

$$V_1 = \frac{m_1 - m_0}{0.789}$$

Porosity rates were further calculated according to the following equation

$$\text{porosity rate } (\%) = \frac{V_1}{V_0} \times 100\%$$

4.3.3. Degradation Profile In Vitro. The degradation profile of scaffolds was assessed according to the percentage of mass remaining after incubation in PBS for a certain period of time. Briefly, the scaffolds were trimmed into cuboids and weighed, which was denoted as m_0. Afterward, the scaffolds were sterilized, transferred into 24-well plates, immersed in 2 mL of PBS, and incubated at 37 °C. The liquid in wells was changed every 2 days. On days 1, 3, 7, 14, 28, 56, and 84, the scaffolds were rinsed with deionized water, freeze-dried, and weighed, which is denoted as m_t. The degradation rates of scaffolds were calculated according to the following equation

$$\text{degradation rate } (\%) = \frac{m_0 - m_t}{m_0} \times 100\%$$

4.4. Scanning Electron Microscopy (SEM). The morphology and microstructure of SBH and PSB scaffolds were characterized by a scanning electron microscope (Philips-FEI, Quanta 200, the Netherlands). The samples were placed on carbon tape and gold-sputtered before observation.

4.5. Chondrocytes Isolation, Proliferation, and Seeding on the Scaffolds. Porcine chondrocytes were isolated from the external ears of three 6-month-old minipigs. All of the procedures were approved by the Ethics Committee of Peking Union Medical College. Briefly, the auricular cartilage was obtained under aseptic condition, fragmented into 1 mm^3 pieces, and digested with 0.25% trypsin for 30 min at 37 °C on a shaker. The fragments were then incubated with 0.2% type IV collagenase for another 8 h under the same condition. Then, the cartilage suspension was screened, centrifuged, and resuspended. The cells were seeded in Petri dishes at a density of 3 × 10^4/mL and cultured in high-glucose Dulbecco's modified Eagle's medium supplemented with 10% FBS and 1 × PSN antibiotic mixture. The culture medium was changed every 2 days. When the cells became 80−90% confluent, they were detached by trypsinization and subcultured in new Petri dishes. The scaffolds were sterilized by γ rays and pretreated by immersion in DMEM for 2 h at 37 °C and 5% CO_2. P2 porcine chondrocytes that reached 80−90% confluence were trypsinized, resuspended, and seeded on scaffolds of two groups, at a density of 3−5 × 10^7/mL and a total volume of 100 μL per scaffold, followed by 4 h incubation to promote cell adhesion. The samples were then cultured in H-DMEM supplemented with 10% FBS and 1 × PSN. The medium was refreshed every 2 days.

4.6. *In Vitro* Biological Evaluations. *4.6.1. Live/Dead Staining.* To detect the cell viability of chondrocytes seeded on the scaffolds, live/dead staining was conducted with the LIVE/DEAD Viability/Cytotoxicity Kit. The scaffolds were incubated with cells for 1, 3, 5, and 7 days after seeding. At each time point mentioned above, the medium was removed, and the samples were rinsed with PBS three times. Calcein AM (5 μL, Component A) and ethidium homodimer-1 (20 μL, Component B) were added to 10 mL of DPBS to obtain the staining solution. The samples were immersed in about 500 μL of staining solution for 30 min under room temperature. The whole process was performed away from light. The samples were rinsed with PBS three times before being observed by an inverted microscope (Nikon ECLIPSE TSl00, Japan).

4.6.2. CCK-8 Assays. Cell viability and proliferation on scaffolds were assessed by cholecystokinin-octapeptide (CCK-8) assays as previously described.[43] Briefly, on days 1, 3, 5, 7, 10, 14, and 21, the culture medium of both constructs was removed and H-DMEM containing 700 μL of 10% CCK-8 solution was then added to each well. After incubation in the dark at 37 °C for 2 h, the medium was aspirated and transferred to 96-well plates. The absorbance of each well at 450 nm was then measured immediately by a microplate reader (PerkinElmer). The measurement of day 1 was set as 100% and the other values were presented as the percentage to day 1 measurement of each group.

4.6.3. SEM Observation of Cell-Laden Scaffolds. Chondrocytes morphology and ECM deposition on scaffolds were observed by SEM after in vitro cultivation for 4 weeks. The cell-laden scaffolds of two groups were washed by PBS and then fixed in PBS solution containing 2.5% glutaraldehyde for 48 h. The samples were then dehydrated by gradient ethanol, dried by critical point drying method, and sprayed with gold before observed by SEM.

4.6.4. Chondrogenesis-Related Gene Expression. The expressions of major chondrogenic markers including *SOX9*, *ACAN*, *COL2A1*, *COL1A1*, *ELN*, and *COMP* were measured by real-time PCR analysis between two groups. The samples

https://dx.doi.org/10.1021/acsomega.0c05890
ACS Omega 2021, 6, 3372−3383

were frozen in liquid nitrogen, ground into a powder, and lysed in TRIzol reagent. Total mRNA was then extracted according to the manufacturer's instructions and quantified using a NanoDrop 2000 spectrophotometer (Thermo Fisher, CA). RNA samples with a 260/280 ratio between 1.8 and 2.0 were reverse-transcribed into single-stranded cDNA according to the manufacturer's protocol (Promega; http://www.promega.com). Real-time PCR was performed using a Light Cycler 480 system with an SYBR green kit (Roche, Germany; http://www.roche.com). The relative expression quantities were calculated using the $2^{-\Delta\Delta Ct}$ method with *GAPDH* as the endogenous reference gene. The forward and reverse primer pairs are listed in Table 1.

4.7. *In Vivo* Chondrogenesis Estimation in Nude Mice. The in vivo compatibility and capability to promote chondrogenesis of both scaffolds were assessed by subcutaneous implantation. After cultured in vitro for 4 weeks, the cell-laden scaffolds were subcutaneously implanted in the back of six female BALB/c nude mice. The applied animals were 5 weeks old, weighed between 28 and 33 g, and randomly divided into two groups. All of the procedures were approved by the Ethics Committee of Peking Union Medical College complied with the guidelines for the care and use of laboratory animals. Standard anesthesia procedure with intraperitoneal injection of pentobarbital sodium (30 mg/kg) was performed before skin incisions were made. For each mouse, two cell-laden scaffolds from PSB scaffolds and SBH scaffolds were subcutaneously implanted in the left- and right-hand sides, respectively, followed by skin suturing. A total of 12 specimens were implanted. All mice were nurtured under IVC condition and on a routine diet, and kept healthy during the whole observation period. The mice were euthanized by cervical dislocation to retrieve the scaffolds for analysis 4 and 16 weeks post surgery. The samples were fixed in 4% paraformaldehyde solution for 48 h, dehydrated in 20% sucrose aqueous solution (w/v), and embedded in an optimum cutting temperature (OCT) compound. Sections of 5 mm thickness were cut and stained with hematoxylin and eosin (H&E). To further evaluate the ECM deposition and cartilage formation, toluidine blue and immunohistochemical (IHC) staining for Collagen I and Collagen II were introduced at both time points. HE and toluidine blue staining were conducted following standard histological techniques. For immunohistochemistry, the sections were pretreated with 10% (v/v) goat serum for 45 min at room temperature and incubated with diluted primary antibody at 4 °C overnight. After careful rinsing, the sections were incubated with a secondary antibody for 2 h at 37 °C. Positive staining was then observed by a DAB detection kit. The sections were counterstained in hematoxylin, mounted with neutral resin, and observed by an optical microscope (Olympus, Japan).

4.8. Statistical Analysis. SPSS 17.0 (IBM) software was applied for data analysis. All quantitative statistics were expressed as mean ± standard error. Statistical analyses between two groups were performed using Student's *t*-test. As for value comparisons among multiple groups, one-way analysis of variance (ANOVA) was conducted for equal variances situations, while Tamhane tests were performed for unequal ones. A significance level was set at 0.05.

■ ASSOCIATED CONTENT

Supporting Information

The Supporting Information is available free of charge at https://pubs.acs.org/doi/10.1021/acsomega.0c05890.

Cell viability and proliferation of chondrocytes on PSB and SBH scaffolds post seeding (PDF)

■ AUTHOR INFORMATION

Corresponding Authors

Zhimin Zhou − *Biomedical Barriers Research Center, Institute of Biomedical Engineering, Chinese Academy of Medical Sciences & Peking Union Medical College, Tianjin 300192, China; Tianjin Key Laboratory of Biomedical Materials, Tianjin 300192, China*; Email: zhouzm@bme.cams.cn

Jincai Fan − *Plastic Surgery Hospital and Institute, Chinese Academy of Medical Sciences & Peking Union Medical College, Beijing 100144, China*; Email: fanjincaimd@hotmail.com

Haiyue Jiang − *Plastic Surgery Hospital and Institute, Chinese Academy of Medical Sciences & Peking Union Medical College, Beijing 100144, China*; orcid.org/0000-0002-8365-5568; Email: jianghy_academy@163.com

Authors

Yan Zeng − *Plastic Surgery Hospital and Institute, Chinese Academy of Medical Sciences & Peking Union Medical College, Beijing 100144, China*

Xiaokai Li − *Biomedical Barriers Research Center, Institute of Biomedical Engineering, Chinese Academy of Medical Sciences & Peking Union Medical College, Tianjin 300192, China; Tianjin Key Laboratory of Biomedical Materials, Tianjin 300192, China*

Xia Liu − *Plastic Surgery Hospital and Institute, Chinese Academy of Medical Sciences & Peking Union Medical College, Beijing 100144, China*

Yuzhou Yang − *Biomedical Barriers Research Center, Institute of Biomedical Engineering, Chinese Academy of Medical Sciences & Peking Union Medical College, Tianjin 300192, China; Tianjin Key Laboratory of Biomedical Materials, Tianjin 300192, China*

Complete contact information is available at: https://pubs.acs.org/10.1021/acsomega.0c05890

Author Contributions

All authors participated in the preparation of this manuscript and approved the final version.

Funding

This work was supported by CAMS Innovation Fund for Medical Sciences (CAMS-I2M-1-007).

Notes

The authors declare no competing financial interest.

■ ABBREVIATIONS

PSB scaffolds, plain silk-based scaffolds; SBH scaffolds, silk-based hybrid scaffolds; PMs, porous microspheres; PLLA, poly-L-lactic acid

■ REFERENCES

(1) Cubitt, J. J.; Chang, L. Y.; Liang, D.; Vandervord, J.; Marucci, D. D. Auricular reconstruction. *J. Paediatr. Child Health* **2019**, *55*, 512−517.

(2) Cao, Y.; Vacanti, J. P.; Paige, K. T.; Upton, J.; Vacanti, C. A. Transplantation of chondrocytes utilizing a polymer-cell construct to produce tissue-engineered cartilage in the shape of a human ear. *Plast. Reconstr. Surg.* **1997**, *100*, 303−304.
(3) Sterodimas, A.; de Faria, J.; Correa, W. E.; Pitanguy, I. Tissue engineering and auricular reconstruction: a review. *J. Plast. Reconstr. Aesthetic Surg* **2009**, *62*, 447−452.
(4) Kang, H.; Lee, S. J.; Ko, I. K.; Kengla, C.; Yoo, J. J.; Atala, A. A 3D bioprinting system to produce human-scale tissue constructs with structural integrity. *Nat. Biotechnol.* **2016**, *34*, 312−319.
(5) Zhang, Y.; Liu, X.; Zeng, L.; Zhang, J.; Zuo, J.; Zou, J.; Ding, J.; Chen, X. Polymer Fiber Scaffolds for Bone and Cartilage Tissue Engineering. *Adv. Funct. Mater.* **2019**, *29*, No. 1903279.
(6) Ribeiro, V. P.; Da Silva Morais, A.; Maia, F. R.; Canadas, R. F.; Costa, J. B.; Oliveira, A. L.; Oliveira, J. M.; Reis, R. L. Combinatory approach for developing silk fibroin scaffolds for cartilage regeneration. *Acta Biomater.* **2018**, *72*, 167−181.
(7) Bružauskaitė, I.; Bironaitė, D.; Bagdonas, E.; Bernotienė, E. Scaffolds and cells for tissue regeneration: different scaffold pore sizes—different cell effects. *Cytotechnology* **2016**, *68*, 355−369.
(8) Lien, S.; Ko, L.; Huang, T. Effect of pore size on ECM secretion and cell growth in gelatin scaffold for articular cartilage tissue engineering. *Acta Biomater.* **2009**, *5*, 670−679.
(9) Yamane, S.; Iwasaki, N.; Kasahara, Y.; Harada, K.; Majima, T.; Monde, K.; Nishimura, S.; Minami, A. Effect of pore size on in vitro cartilage formation using chitosan-based hyaluronic acid hybrid polymer fibers. *J. Biomed. Mater. Res., Part A* **2007**, *81*, 586−593.
(10) Yan, D.; Zhou, G.; Zhou, X.; Liu, W.; Zhang, W. J.; Luo, X.; Zhang, L.; Jiang, T.; Cui, L.; Cao, Y. The impact of low levels of collagen IX and pyridinoline on the mechanical properties of in vitro engineered cartilage. *Biomaterials* **2009**, *30*, 814−821.
(11) Discher, D. E.; Janmey, P.; Wang, Y. L. Tissue cells feel and respond to the stiffness of their substrate. *Science* **2005**, *310*, 1139−1143.
(12) Jukola, H.; Nikkola, L.; Gomes, M. E.; Chiellini, F.; Tukiainen, M.; Kellomäki, M.; Chiellini, E.; Reis, R. L.; Ashammakhi, N. Development of a bioactive glass fiber reinforced starch polycaprolactone composite. *J. Biomed. Mater. Res., Part B* **2008**, *87*, 197−203.
(13) Mandal, B. B.; Grinberg, A.; Gil, E. S.; Panilaitis, B.; Kaplan, D. L. High-strength silk protein scaffolds for bone repair. *Proc. Natl. Acad. Sci. U.S.A.* **2012**, *109*, 7699−7704.
(14) Yodmuang, S.; McNamara, S. L.; Nover, A. B.; Mandal, B. B.; Agarwal, M.; Kelly, T. N.; Chao, P. G.; Hung, C.; Kaplan, D. L.; Vunjak-Novakovic, G. Silk microfiber-reinforced silk hydrogel composites for functional cartilage tissue repair. *Acta Biomater.* **2015**, *11*, 27−36.
(15) Singh, Y. P.; Adhikary, M.; Bhardwaj, N.; Bhunia, B. K.; Mandal, B. B. Silk fiber reinforcement modulates in vitro chondrogenesis in 3D composite scaffolds. *Biomed. Mater.* **2017**, *12*, No. 45012.
(16) Mobini, S.; Hoyer, B.; Solati-Hashjin, M.; Lode, A.; Nosoudi, N.; Samadikuchaksaraei, A.; Gelinsky, M. Fabrication and characterization of regenerated silk scaffolds reinforced with natural silk fibers for bone tissue engineering. *J. Biomed. Mater. Res., Part A* **2013**, *101*, 2392−2404.
(17) Mobini, S.; Taghizadeh-Jahed, M.; Khanmohammadi, M.; Moshiri, A.; Naderi, M. M.; Heidari-Vala, H.; Ashrafi, H. J.; Khanjani, S.; Springer, A.; Akhondi, M. M.; et al. Comparative evaluation of in vivo biocompatibility and biodegradability of regenerated silk scaffolds reinforced with/without natural silk fibers. *J. Biomater. Appl.* **2016**, *30*, 793−809.
(18) Wang, J.; Sun, X.; Zhang, Z.; Wang, Y.; Huang, C.; Yang, C.; Liu, L.; Zhang, Q. Silk fibroin/collagen/hyaluronic acid scaffold incorporating pilose antler polypeptides microspheres for cartilage tissue engineering. *Mater. Sci. Eng., C* **2019**, *94*, 35−44.
(19) Wen, Y.; Dai, N.; Hsu, S. Biodegradable water-based polyurethane scaffolds with a sequential release function for cell-free cartilage tissue engineering. *Acta Biomater.* **2019**, *88*, 301−313.
(20) Cao, H.; Chen, M.; Liu, Y.; Liu, Y.; Huang, Y.; Wang, J.; Chen, J.; Zhang, Q. Fish collagen-based scaffold containing PLGA microspheres for controlled growth factor delivery in skin tissue engineering. *Colloids Surf., B* **2015**, *136*, 1098−1106.
(21) Huang, W.; Shi, X.; Ren, L.; Du, C.; Wang, Y. PHBV microspheres−PLGA matrix composite scaffold for bone tissue engineering. *Biomaterials* **2010**, *31*, 4278−4285.
(22) Li, C.; Zhang, J.; Li, Y.; Moran, S.; Khang, G.; Ge, Z. Poly (l-lactide-co-caprolactone) scaffolds enhanced with poly (beta-hydroxybutyrate-co-beta-hydroxyvalerate) microspheres for cartilage regeneration. *Biomed. Mater.* **2013**, *8*, No. 25005.
(23) Edwards, D. A.; Hanes, J.; Caponetti, G.; Hrkach, J.; Ben-Jebria, A.; Eskew, M. L.; Mintzes, J.; Deaver, D.; Lotan, N.; Langer, R. Large porous particles for pulmonary drug delivery. *Science* **1997**, *276*, 1868−1871.
(24) Chung, H. J.; Kim, I. K.; Kim, T. G.; Park, T. G. Highly Open Porous Biodegradable Microcarriers:In Vitro Cultivation of Chondrocytes for Injectable Delivery. *Tissue Eng., Part A* **2008**, *14*, 607−615.
(25) Jin, G.; Kim, H. Porous microcarrier-enabled three-dimensional culture of chondrocytes for cartilage engineering: A feasibility study. *Tissue Eng. Regen. Med.* **2016**, *13*, 235−241.
(26) Tan, Y. J.; Tan, X.; Yeong, W. Y.; Tor, S. B. Hybrid microscaffold-based 3D bioprinting of multi-cellular constructs with high compressive strength: A new biofabrication strategy. *Sci. Rep.* **2016**, No. 39140.
(27) Zhou, G.; Jiang, H.; Yin, Z.; Liu, Y.; Zhang, Q.; Zhang, C.; Pan, B.; Zhou, J.; Zhou, X.; Sun, H.; et al. In Vitro Regeneration of Patient-specific Ear-shaped Cartilage and Its First Clinical Application for Auricular Reconstruction. *EBioMedicine* **2018**, *28*, 287−302.
(28) Ding, J.; Chen, B.; Lv, T.; Liu, X.; Fu, X.; Wang, Q.; Yan, L.; Kang, N.; Cao, Y.; Xiao, R. Bone Marrow Mesenchymal Stem Cell-Based Engineered Cartilage Ameliorates Polyglycolic Acid/Polylactic Acid Scaffold-Induced Inflammation Through M2 Polarization of Macrophages in a Pig Model. *Stem Cells Transl. Med.* **2016**, *5*, 1079−1089.
(29) Ju, H. W.; Sheikh, F. A.; Moon, B. M.; Park, H. J.; Lee, O. J.; Kim, J. H.; Eun, J. J.; Khang, G.; Park, C. H. Fabrication of poly(lactic-co-glycolic acid) scaffolds containing silk fibroin scaffolds for tissue engineering applications. *J. Biomed. Mater. Res., Part A* **2014**, *102*, 2713−2724.
(30) Bos, E. J.; Pluemeekers, M.; Helder, M.; Kuzmin, N.; van der Laan, K.; Groot, M.; van Osch, G.; van Zuijlen, P. Structural and Mechanical Comparison of Human Ear, Alar, and Septal Cartilage. *Plast. Reconstr. Surg.* **2018**, *6*, No. e1610.
(31) Nimeskern, L.; Utomo, L.; Lehtoviita, I.; Fessel, G.; Snedeker, J. G.; van Osch, G. J. V. M.; Müller, R.; Stok, K. S. Tissue composition regulates distinct viscoelastic responses in auricular and articular cartilage. *J. Biomech.* **2016**, *49*, 344−352.
(32) Cholas, R.; Kunjalukkal Padmanabhan, S.; Gervaso, F.; Udayan, G.; Monaco, G.; Sannino, A.; Licciulli, A. Scaffolds for bone regeneration made of hydroxyapatite microspheres in a collagen matrix. *Mater. Sci. Eng., C* **2016**, *63*, 499−505.
(33) Nava, M. M.; Draghi, L.; Giordano, C.; Pietrabissa, R. The effect of scaffold pore size in cartilage tissue engineering. *J. Appl. Biomater. Funct.* **2016**, *14*, e223−e229.
(34) Zhang, Q.; Lu, H.; Kawazoe, N.; Chen, G. Pore size effect of collagen scaffolds on cartilage regeneration. *Acta Biomater.* **2014**, *10*, 2005−2013.
(35) Freedman, B. R.; Mooney, D. J. Biomaterials to Mimic and Heal Connective Tissues. *Adv. Mater.* **2019**, *31*, No. 1806695.
(36) Zhang, L.; He, A.; Yin, Z.; Yu, Z.; Luo, X.; Liu, W.; Zhang, W.; Cao, Y.; Liu, Y.; Zhou, G. Regeneration of human-ear-shaped cartilage by co-culturing human microtia chondrocytes with BMSCs. *Biomaterials* **2014**, *35*, 4878−4887.
(37) Fazal, N.; Latief, N. Bombyx mori derived scaffolds and their use in cartilage regeneration: a systematic review. *Osteoarthritis Cartilage* **2018**, *26*, 1583−1594.

https://dx.doi.org/10.1021/acsomega.0c05890
ACS Omega 2021, 6, 3372−3383

(38) Nichol, J. W.; Koshy, S. T.; Bae, H.; Hwang, C. M.; Yamanlar, S.; Khademhosseini, A. Cell-laden microengineered gelatin methacrylate hydrogels. *Biomaterials* **2010**, *31*, 5536−5544.
(39) Xue, J.; Wu, T.; Qiu, J.; Rutledge, S.; Tanes, M. L.; Xia, Y. Promoting Cell Migration and Neurite Extension along Uniaxially Aligned Nanofibers with Biomacromolecular Particles in a Density Gradient. *Adv. Funct. Mater.* **2020**, *n/a*, No. 2002031.
(40) Wang, Y.; Blasioli, D. J.; Kim, H. J.; Kim, H. S.; Kaplan, D. L. Cartilage tissue engineering with silk scaffolds and human articular chondrocytes. *Biomaterials* **2006**, *27*, 4434−4442.
(41) Huh, Y. H.; Ryu, J.; Chun, J. Regulation of Type II Collagen Expression by Histone Deacetylase in Articular Chondrocytes. *J. Biol. Chem.* **2007**, *282*, 17123−17131.
(42) Ghayor, C.; Chadjichristos, C.; Herrouin, J.; Ala-Kokko, L.; Suske, G.; Pujol, J.; Galéra, P. SP3 Represses the SP1-mediated Transactivation of the Human COL2A1 Gene in Primary and Dedifferentiated Chondrocytes. *J. Biol. Chem.* **2001**, *276*, 36881−36895.
(43) Wang, Y.; Bella, E.; Lee, C. S. D.; Migliaresi, C.; Pelcastre, L.; Schwartz, Z.; Boyan, B. D.; Motta, A. The synergistic effects of 3-D porous silk fibroin matrix scaffold properties and hydrodynamic environment in cartilage tissue regeneration. *Biomaterials* **2010**, *31*, 4672−4681.

https://dx.doi.org/10.1021/acsomega.0c05890
ACS Omega 2021, 6, 3372−3383